

See discussions, stats, and author profiles for this publication at: <https://www.researchgate.net/publication/232743533>

# Experimental Study of Carbon Black and Diesel Engine Soot Oxidation Kinetics Using Thermogravimetric Analysis

ARTICLE in ENERGY & FUELS · AUGUST 2012

Impact Factor: 2.79 · DOI: 10.1021/ef3009025

---

CITATIONS

15

READS

130

## 5 AUTHORS, INCLUDING:



[Hom Sharma](#)

Lawrence Livermore National Laboratory

20 PUBLICATIONS 51 CITATIONS

[SEE PROFILE](#)



[Lakshitha Pahalagedara](#)

University of Connecticut

16 PUBLICATIONS 114 CITATIONS

[SEE PROFILE](#)



[Steven L Suib](#)

University of Connecticut

652 PUBLICATIONS 15,517 CITATIONS

[SEE PROFILE](#)



[Ashish Mhadeshwar](#)

ExxonMobil

19 PUBLICATIONS 644 CITATIONS

[SEE PROFILE](#)

# Experimental Study of Carbon Black and Diesel Engine Soot Oxidation Kinetics Using Thermogravimetric Analysis

Hom N. Sharma,<sup>†,‡</sup> Lakshitha Pahalagedara,<sup>§</sup> Ameya Joshi,<sup>||</sup> Steven L. Suib,<sup>§</sup> and Ashish B. Mhadeshwar<sup>\*,†,‡</sup>

<sup>†</sup>Department of Chemical, Materials, and Biomolecular Engineering, University of Connecticut, 191 Auditorium Road, Unit 3222, Storrs, Connecticut 06269, United States

<sup>‡</sup>Center for Clean Energy Engineering, University of Connecticut, 44 Weaver Road, Unit 5233, Storrs, Connecticut 06268, United States

<sup>§</sup>Department of Chemistry, University of Connecticut, 55 North Eagleville Road, Unit 3060, Storrs, Connecticut 06269, United States

<sup>||</sup>Corning, Incorporated, Science Center Road, SP TD 01-1, Corning, New York 14831, United States

**ABSTRACT:** Non-catalytic oxidation kinetics of diesel engine soot and more than a dozen commercial carbon black samples was investigated using non-isothermal and isothermal thermogravimetric analysis (TGA) experiments. The effect of various operating parameters, such as oxygen flow rate, initial sample mass, oxygen partial pressure, crucible type, and ramp rate, on the oxidation rate was investigated. Three types of TGA experiments (non-isothermal single-ramp rate, non-isothermal multiple-ramp rates, and isothermal) were conducted and analyzed to extract the kinetic parameters for oxidation. Activation energies for oxidation of carbon black samples ranged from 125 to 257 kJ/mol, whereas that for soot oxidation was ~155 kJ/mol. Furthermore, oxidation rate trends were explained on the basis of structural characteristics, such as scanning electron microscopy (SEM)-based average particle size and Brunauer–Emmett–Teller (BET) surface area. In general, a low particle size and high surface area were associated with a higher oxidation rate and vice versa. A thorough understanding of the non-catalytic oxidation kinetics developed in this work along with the correlation of the oxidation rate with the structural parameters may assist in efficient oxidation of diesel engine soot during the regeneration of diesel particulate filters.

## 1. INTRODUCTION

More than 13 million diesel vehicles are responsible for transportation of 94% of the goods in the U.S. and use ~4 million barrels of diesel per day.<sup>1–3</sup> In the European market, 53% of the passenger cars run on diesel.<sup>4</sup> Diesel engines are the workhorses for industrial, commercial, and personal transportation and also play a vital role in power generation, because of the highly efficient combustion, excellent fuel economy, torque, durability, reliability, and low operating costs.<sup>5–7</sup> However, emissions from diesel engines contain fine particles produced during high-temperature pyrolysis or combustion. Diesel particulate matter (PM), also known as soot, is primarily composed of carbon along with some organic compounds, inorganic compounds (ash), sulfur compounds, and traces of metals from unburnt fuel and lubricating oil. PM formation is a complex phenomenon, which depends upon the engine operating conditions, fuel type, and lubricating oil, resulting in a wide range of particle sizes and chemical compositions.<sup>8–11</sup> PM emissions are responsible for various human health and environmental problems, such as asthma, bronchitis, lung cancer, air pollution, and global warming.<sup>5,12,13</sup> Diesel particulate filter (DPF) is the most popular aftertreatment technology to meet the stringent PM emission standards.<sup>14,15</sup> DPFs need to be periodically regenerated through oxidation of soot; otherwise, the accumulated soot can cause backpressure, resulting in decreased fuel economy and possible engine and/or filter failure.<sup>16,17</sup> Given the complexity and variability in the soot structure as well as the need for periodic DPF

regeneration, there is an urgent need to develop a comprehensive understanding for the kinetics of soot oxidation.

This work focused on developing such an understanding through a comprehensive investigation of 15 carbonaceous samples (diesel engine soot provided by Corning, 13 commercial carbon black samples, and graphite). The effect of various parameters, such as the oxidizer flow rate, initial sample mass, partial pressure of oxygen, crucible type, and ramp rate, was studied using temperature-programmed oxidation (TPO) thermogravimetric experiments. The paper is organized as follows. First, experimental details are provided in section 2, followed by a description of the data analysis methods in section 3. In section 4, we discuss the effect of various operating conditions in non-isothermal experiments, followed by kinetic parameter extraction. The results are compared to isothermal experiments presented in section 5. Summary and concluding remarks are presented in the end.

## 2. EXPERIMENTAL SECTION

**2.1. Materials.** A total of 15 different samples studied included a diesel engine soot sample provided by Corning, 13 commercial carbon black samples obtained from various manufacturers, and a graphitic carbon sample. The samples were as follows: (1) diesel soot (Corning), (2) graphite (Fisher Scientific), (3) Mogul-E (Cabot), (4) Monarch 1300 (Cabot), (5) Monarch 1400 (Cabot), (6) Monarch 280 (Cabot),

Received: May 24, 2012

Revised: August 2, 2012

Published: August 3, 2012



(7) N 120 (Continental carbon), (8) N 339 (Continental carbon), (9) N 762 (Continental carbon), (10) Printex-G (Orion), (11) Printex-U (Orion), (12) Printex-XE2B (Orion), (13) Regal 330 R (Cabot), (14) Regal 400 R (Cabot), and (15) VulcanXC72R (Cabot). Throughout the paper, the samples are referred in this order. Two of the samples (Monarch 1300 and Monarch 1400) contained 7% moisture, as compared to negligible moisture (0–0.6%) in the other samples.

**2.2. Thermogravimetric Analysis (TGA).** A TGA Q5000 IR thermogravimetric analyzer from TA Instruments was used for all of the experiments. This is a thermal weight-change analysis instrument, used in conjunction with a controller computer and associated software to make up a thermal analysis system. This TGA is also equipped with an autosampler for multiple sample loadings. In this work, we developed mixed methods consisting of non-isothermal and isothermal steps. Instrumental specifications and experimental protocol details are given in Table 1.

**Table 1. Details of the TGA Instrument and Experimental Protocols**

Technical Specifications <sup>79</sup>		
weighting capacity	100 mg	
weighting precision	±0.01%	
sensitivity	<0.1 µg (1 ppm)	
signal resolution	0.002 µg	
temperature range	ambient to 1200 °C	
furnace type	infrared heating with a built-in electromagnetic coil for automated temperature calibration	
isothermal temperature accuracy	±1 °C	
isothermal temperature precision	±0.1 °C	
linear heating rates	0.1–500 °C/min in 0.01 °C/min increments	
special heating mode	hi-res TGA and modulated TGA	
autosampler	16 sample carousel with automated pan punching	
Experimental Protocol for Non-isothermal Tests		
step	description	stage
1	flow of oxidant gas with nitrogen	initial
2	ramp to 800 °C with ramp rate β = 5–20 °C/min	heating
3	hold at 800 °C for 15 min	isothermal
4	cool to room temperature	cooling
Experimental Protocol for Isothermal Tests		
step	description	stage
1	flow of nitrogen (balance and purge gases)	initial
2	ramp to $T_{\text{isothermal}}$ with β = 20 °C/min	heating
3	flow of oxidant gas with nitrogen	isothermal
4	hold at $T_{\text{isothermal}}$ for 120 min	isothermal
5	cool to room temperature	cooling

In all of the experiments, the oxidizer gas (UHP air or 10% O<sub>2</sub> in Ar from Airgas) flow rate was 60 mL/min and N<sub>2</sub> was used as a purge gas with a flow rate of 40 mL/min. The initial mass of the carbon black samples was ~10–12 mg. However, because of the low density of diesel soot, an initial mass of only ~2.5 mg was used. For the non-isothermal experiments, the samples were heated in a platinum (Pt) crucible (the Pt crucible was inert, as discussed later in section 2.3.4) from room temperature to 800 °C at a chosen ramp rate (5–20 °C/min), followed by a 15 min hold at 800 °C, and then cooling back to room temperature. For the isothermal experiments, first, the samples were heated to the desired temperature with a ramp rate of 20 °C/min, and then, the samples were kept at the isothermal point for 2 h under oxidizing environment, followed by cooling back to room temperature. Non-isothermal tests are typically preferred over isothermal tests for two reasons: (i) an isothermal test always consists of a finite non-

isothermal heating time, as a result of which strictly isothermal tests are not possible,<sup>18</sup> and (ii) multiple experiments are required for extraction of kinetic parameters from isothermal tests.<sup>19,20</sup> On the other hand, isothermal tests provide information about the characteristic profile of the reaction and, hence, provide an idea about the appropriate kinetic model.<sup>18</sup> In this work, we conducted isothermal tests for selected samples to extract the kinetic parameters and to validate the parameters obtained from the non-isothermal experiments.

Finally, the oxidation rate is defined on the basis of the temperature required for a certain level of fractional conversion. For example,  $T_{10}$ ,  $T_{50}$ , and  $T_{90}$  represent the temperatures required to achieve 10, 50, and 90% mass loss, respectively.  $T_{10}$  is also referred to as the light-off temperature.

### 2.3. Factors Affecting TGA Experiments. 2.3.1. Oxygen Flow Rate.

The overall efficiency of the gas–solid reactions can be greatly affected by the gas flow rate and, hence, mass-transfer limitations or limiting reactants.<sup>19–23</sup> For the oxidation of carbon black or soot, the availability of oxygen is critical; otherwise, the observed oxidation efficiency may be lower because of the lack of sufficient oxygen. This is particularly important at high temperatures, where the soot oxidation rate is high and the lack of oxygen can limit the overall soot oxidation rate. To ensure that the TGA experiments reported here were not affected by such limitations because of insufficient availability of oxygen in the oxidizer gas, we conducted a series of experiments with various oxidizer gas flow rates while maintaining other parameters the same. Figure 1 shows the mass loss profile of Printex-U for various levels

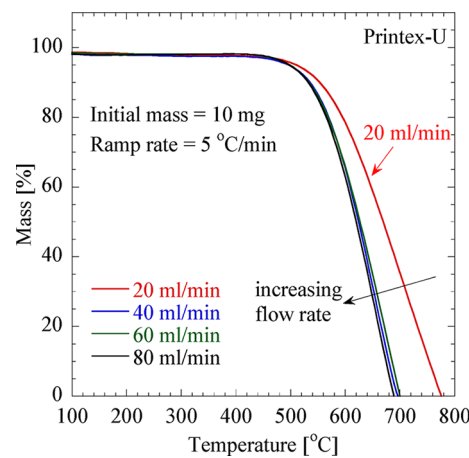


**Figure 1.** Oxidation profile of Printex-U with different flow rates of air. Operating conditions: non-isothermal experiment, initial mass of 10 mg, and ramp rate at 5 °C/min. Data indicate that the gas flow rate must be at least 40 mL/min to avoid the limitations associated with the availability of oxygen.

of air flow rates (20–80 mL/min). The oxidation rate at a gas flow rate of 20 mL/min was lower than that at a gas flow rate of 40 mL/min or higher, but the rate stayed constant for gas flow rates of 40 mL/min and higher. Therefore, the oxidizer gas flow rate must be at least 40 mL/min to avoid the scenario in which oxygen becomes the limiting reactant. On the basis of these experiments, we used an oxidizer gas flow rate of 60 mL/min in all of the TGA experiments reported in this paper.

**2.3.2. Initial Sample Mass.** TGA analysis is also affected, to some extent, by the initial sample mass used in the experiment.<sup>23,24</sup> A large initial mass may be associated with diffusional limitations,<sup>24–27</sup> whereas a small initial mass may result in increased uncertainty along with low reproducibility.<sup>20</sup> Furthermore, a large initial mass may cause self-heating (exothermic) and self-cooling (endothermic), producing a large deviation from the programmed heating rates.<sup>28</sup> The temperature gradient could be created as a result of the low thermal conductivity of the samples, producing regions with different temperatures.<sup>28</sup> As shown in Figure 2, we conducted multiple experiments with different initial masses and ramp rates (5–20 °C/min) for Printex-U (panel a, 2–20 mg) and Printex-XE2B (panel b, 8–14 mg; panel c, 4–14 mg; and

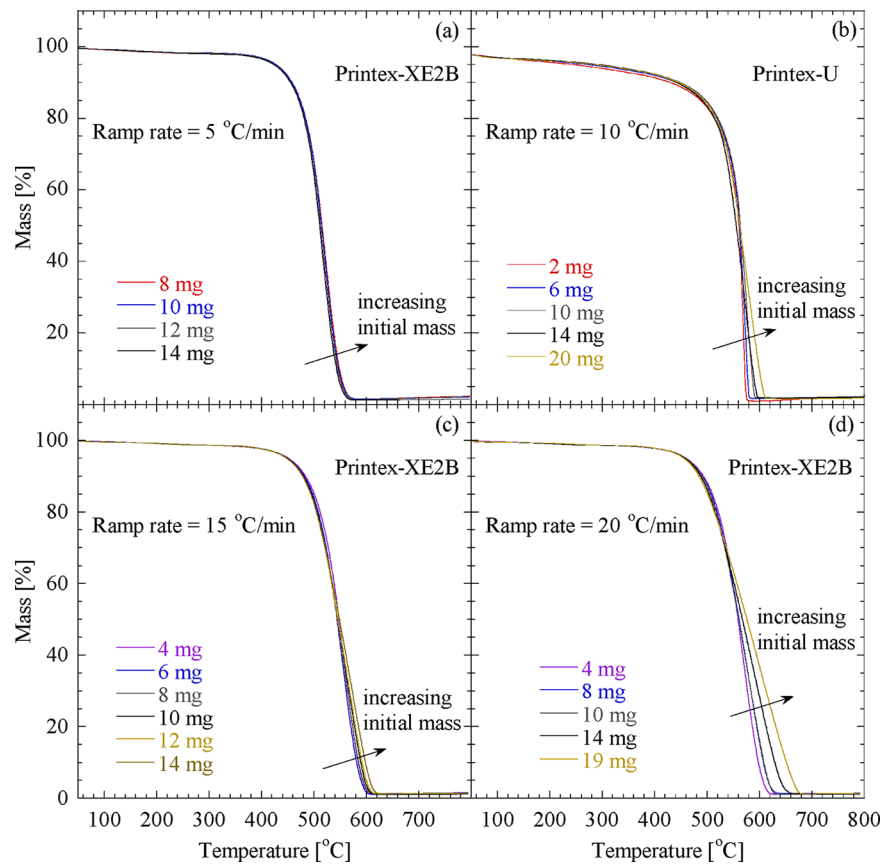


**Figure 2.** Effect of the initial sample mass and ramp rate on the oxidation of (a) Printex-XE2B with a ramp rate of 5 °C/min and an initial mass of 8–14 mg, (b) Printex-U with a ramp rate of 10 °C/min and an initial mass of 2–20 mg, (c) Printex-XE2B with a ramp rate of 15 °C/min and an initial mass of 4–14 mg, and (d) Printex-XE2B with a ramp rate of 20 °C/min and an initial mass of 4–19 mg. Operating conditions: non-isothermal experiment, air oxidant, and flow rate at 60 mL/min.

panel d, 4–19 mg). We observed that large initial masses were affected by diffusional limitations, as evident from the delayed oxidation rate. On the basis of these experiments, we selected moderate initial masses of 10–12 mg for each sample, except for diesel soot (~2.5 mg), which had a much lower density.

**2.3.3. Ramp Rate.** The effect of the ramp rate on gas–solid reactions is well-documented in the literature.<sup>29–34</sup> High ramp rates are typically associated with heat- and mass-transfer limitations.<sup>33</sup> On the other hand, experiments conducted with low ramp rates are not influenced by such limitations.<sup>35</sup> Our results in Figure 2 for different initial masses and ramp rates showed delayed oxidation rates in the case of large initial masses and high ramp rates as a result of their combined effect (e.g., Figure 2d). However, in general, the effect of the initial mass was negligible in the considered initial mass range, with a ramp rate of 5–15 °C/min. On the basis of these experiments, we have chosen a low ramp rate of 5 °C/min for most of the experiments.

**2.3.4. Crucible.** The crucible shape in the TGA experiments can significantly influence the oxidation kinetics because of mass-transfer limitations.<sup>20,23,26,27,36</sup> A large crucible height can lead to a large stagnant volume (space available in the crucible above the sample) and, hence, diffusion limitations.<sup>20,23,27,36</sup> Therefore, short and wide crucibles are typically recommended for such studies.<sup>23,37</sup> In this work, we used short and wide crucibles ( $D = 10$  mm,  $h = 2$  mm, and  $h/D = 0.2$ , with actual sample  $h/D < 0.2$ ) to avoid such limitations. Furthermore, to ensure that the Pt crucible is inert in the oxidation experiments, we conducted additional experiments with an alumina crucible in identical operating conditions. As shown in Figure 3, results with both crucibles were almost identical for two samples (panel a, Printex-XE2B; panel b, Printex-U); hence, the Pt crucible could be considered as inert in the subsequent experiments.

**2.3.5. Diffusion Limitations.** Diffusion limitations in soot oxidation kinetics during TGA experiments have been discussed in the literature,<sup>20,23–25,27,30,36,38–43</sup> and such limitations can impact kinetic parameter estimation.<sup>24,27,38,40,43</sup> As discussed earlier, diffusion limitations can be avoided or minimized by selecting an appropriate initial sample mass, ramp rate, crucible shape, sample packing, bed height, and stagnation volume.<sup>23,24,27,36,38,44</sup> Internal mass-transfer limitations could also be important and could differ for each sample because of different pore sizes. Such limitations have been estimated in the literature using the effectiveness factor and Thiele modulus;<sup>40,45,46</sup> however, they were not considered in the scope of our work presented here.

**2.4. Experimental Reproducibility.** Prior to discussing the results and data analysis from the TGA experiments for multiple samples and various operating conditions, it was important to ensure that the experiments had good reproducibility. Figure 4 shows an example of the experimental reproducibility over three runs for the oxidation of diesel soot (panel a) and Printex-XE2B (panel b). As observed from the overlapping profiles, the TGA experiments were highly reproducible.

### 3. DATA ANALYSIS FOR KINETIC PARAMETER EXTRACTION

Three methods were used for the TGA data analysis: (a) non-isothermal single-ramp rate, (b) non-isothermal multiple-ramp rates, and (c) isothermal. A majority of the results presented in this work are focused around the non-isothermal single-ramp rate method, whereas the other two methods are demonstrated for additional validation or comparison. Next, we discuss the details of the data analysis for the three methods.

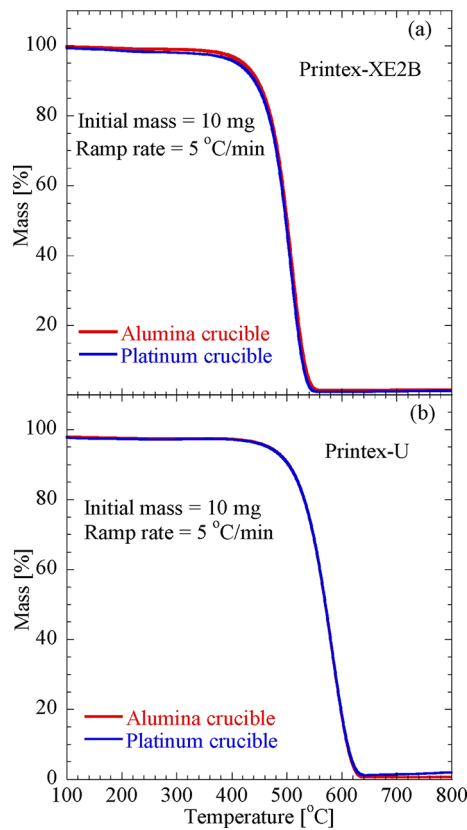


**Figure 3.** Effect of the crucible type on the oxidation of (a) Printex-XE2B with a ramp rate of 5 °C/min and an initial mass of 10 mg and (b) Printex-U with a ramp rate of 5 °C/min and an initial mass of 10 mg. Operating conditions: non-isothermal experiment, air oxidant, and flow rate at 60 mL/min.

### 3.1. Method A: Non-isothermal Single-Ramp Rate Method.

Estimation of kinetic parameters from TGA data can be performed using various approaches, as recommended by the Kinetics Committee of the International Confederation for Thermal Analysis and Calorimetry (ICTAC).<sup>18</sup> However, the most widely used approach for kinetic parameter estimation from soot or carbon black oxidation is based on the Arrhenius equation format<sup>20,47,48</sup>

$$-\frac{dm}{dt} = km^n p_{O_2}^r = A \exp\left(-\frac{E_a}{RT}\right) m^n p_{O_2}^r \quad (1)$$

where  $m$  is the instantaneous sample mass at time  $t$ ,  $k$  is the reaction rate constant,  $A$  is the pre-exponential factor,  $E_a$  is the activation energy,  $T$  is the operating temperature,  $p_{O_2}$  is the partial pressure of oxygen, and  $n$  and  $r$  are the reaction orders for carbon and oxygen, respectively. It is known that the surface area of the carbonaceous samples increases during oxidation.<sup>9</sup> However, any change in the surface area and pore size effects is not accounted for in the simplified kinetic expression. Furthermore, most literature studies for carbon black or soot oxidation show reaction orders close to unity<sup>20,25,39,40</sup> (see section 5 for the validity of this assumption). In that case, the above equation can be rearranged as

$$\ln\left(-\frac{dm}{mdt}\right) = \ln(Ap_{O_2}) - \frac{E_a}{RT} \quad (2)$$

where  $E_a$  and  $A$  can be estimated from the slope and intercept of a  $\ln(-dm/mdt)$  against  $1/T$  plot. In this method, TGA data

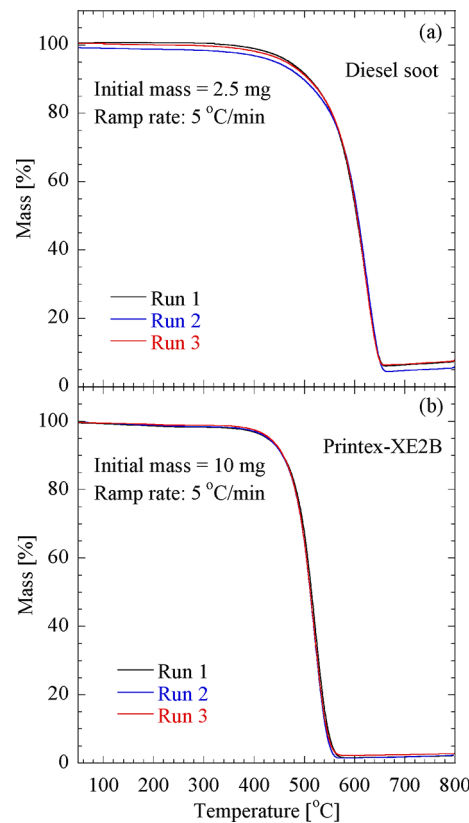


**Figure 4.** Reproducibility of the TGA experiments for (a) diesel soot with an initial mass of 2.5 mg and (b) Printex-XE2B with an initial mass of 10 mg. Operating conditions: non-isothermal experiment, air oxidant, flow rate at 60 mL/min, and ramp rate at 5 °C/min.

at a single-ramp rate are sufficient for the analysis and kinetic parameter extraction.

### 3.2. Method B: Non-isothermal Multiple-Ramp Rate Method.

To delineate the effect of the ramp rate from the kinetic parameters, they can also be estimated using a fractional conversion  $\alpha$  [where  $\alpha = 1 - (m/m_0)$ ] in the non-isothermal experiments conducted at different ramp rates  $\beta$ . This analysis is based on the Flynn–Wall–Ozawa method<sup>49–52</sup> and Doyle's approximation.<sup>53,54</sup> Equation 1 can be written in terms of fractional conversion  $\alpha$  as

$$\begin{aligned} \frac{d\alpha}{dt} &= -\frac{1}{m_0} \frac{dm}{dt} \\ &= A \exp\left(-\frac{E_a}{RT}\right) \frac{m}{m_0} p_{O_2} \\ &= A \exp\left(-\frac{E_a}{RT}\right) (1 - \alpha) p_{O_2} \end{aligned} \quad (3)$$

With a linear ramp rate  $\beta = dT/dt$ , eq 3 can be written as

$$\frac{d\alpha}{dT} = \frac{A}{\beta} \exp\left(-\frac{E_a}{RT}\right) (1 - \alpha) p_{O_2} \quad (4)$$

Integrating this equation from a very low temperature (zero conversion) to the final temperature  $T$ , corresponding to a final degree of conversion  $\alpha$ , and using  $x = E_a/RT$  gives

$$-\ln(1 - \alpha) = \frac{Ap_{O_2} E_a}{\beta R} \int_x^\infty \frac{e^{-x}}{x^2} dx = \frac{Ap_{O_2} E_a}{\beta R} I(x) \quad (5)$$

The integral  $I(x)$  is approximated as<sup>28,51</sup>

$$\log I(x) \approx -2.315 - 0.457x \quad (6)$$

When eqs 5 and 6 are combined and rearranged, we obtain

$$\log \beta = \log \left( \frac{Ap_{O_2} E_a / R}{-\ln(1 - \alpha)} \right) - 2.315 - 0.457 \frac{E_a}{RT} \quad (7)$$

The activation energy  $E_a$  for different conversion values  $\alpha$  can be calculated from the slope of a  $\log \beta$  versus  $1/T$  plot.

**3.3. Method C: Isothermal Method.** Isothermal tests provide another way of studying the kinetics of gas–solid reactions occurring in carbon black or soot oxidation.<sup>12,23,30,55–57</sup>

Starting from eq 1, under isothermal conditions, one can write

$$\begin{aligned} \ln(1 - \alpha) &= \ln \left( \frac{m}{m_0} \right) \\ &= \int_{m_0}^m \frac{dm}{m} \\ &= \int_0^t -A \exp \left( -\frac{E_a}{RT} \right) p_{O_2} dt \\ &= -A \exp \left( -\frac{E_a}{RT} \right) p_{O_2} t \end{aligned} \quad (8)$$

When eq 8 is rearranged, we obtain

$$-\ln t = \ln \left[ \frac{Ap_{O_2}}{-\ln(1 - \alpha)} \right] - \frac{E_a}{RT} \quad (9)$$

A plot of  $-\ln t$  versus  $1/T$  at a chosen value of  $\alpha$  gives the activation energy  $E_a$  from the slope and pre-exponential factor  $A$  from the intercept.<sup>28</sup>

Given the assumptions associated with eqs 1 and 2, the kinetic parameters (activation energies and pre-exponential factors) estimated using the aforementioned methods should be treated as apparent parameters only.

#### 4. OXIDATION KINETICS USING NON-ISOTHERMAL EXPERIMENTS

**4.1. Effect of the Oxygen Partial Pressure.** Soot could be oxidized using the oxygen present in the diesel engine exhaust (5–15% oxygen<sup>58,59</sup>) or using air. Although the oxygen content in air is higher than that in the typical diesel engine exhaust, literature studies have commonly used air to test the oxidation of soot samples.<sup>20,55,60</sup> Therefore, we conducted the TGA experiments with both oxidizers: (i) 10%  $O_2$  in Ar and (ii) air. Experimental protocol details are provided in Table 1. Mass loss profiles for all 15 samples with these two oxidizers are shown in Figures 5 and 6, respectively, with a constant ramp rate of 5 °C/min. The diesel soot sample in this study was collected under real diesel engine exhaust conditions [engine type, light duty; engine swept volume, 2 L; revolutions per minute (rpm), 3250 min<sup>-1</sup>; torque, 50 N m; power, 17 kW; and exhaust gas flow rate, 253 kg/h]. It contained metal oxides and ash particles, which were not burnt off during the oxidation experiments. A very small amount of ash particles was observed in the crucible after the diesel soot experiments, which was not the case with other carbon black samples. Therefore, the diesel soot conversion was not 100%, even at high temperatures, as observed in Figures 5 and 6. The negligible deviation from

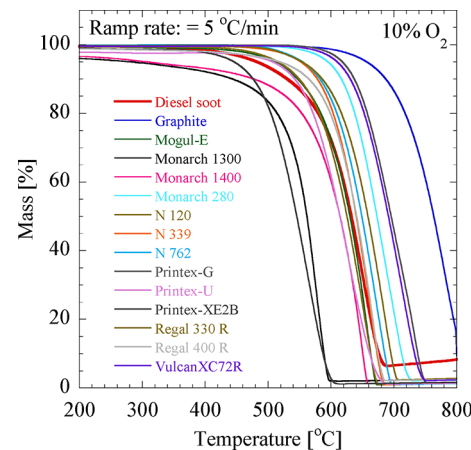


**Figure 5.** Mass loss profiles of all samples with 10%  $O_2$ . Operating conditions: non-isothermal experiment, initial mass range of 2.5–12 mg, flow rate at 60 mL/min, and ramp rate at 5 °C/min. Diesel soot showed incomplete conversion because of the presence of metal oxides and ash particles.

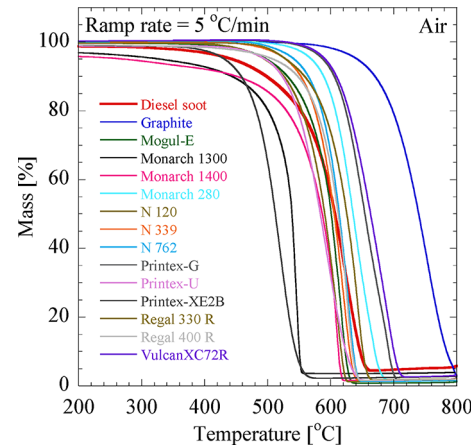


**Figure 6.** Mass loss profiles of all samples with air. Operating conditions: non-isothermal experiment, initial mass range of 2.5–12 mg, flow rate at 60 mL/min, and ramp rate at 5 °C/min. Diesel soot showed incomplete conversion because of the presence of metal oxides and ash particles.

100% conversion for other samples and the slight increase in diesel soot mass with the temperature (at high temperatures) could be associated with experimental uncertainty in measuring very small quantities.

Details of  $T_{10}$ ,  $T_{50}$ , and  $T_{90}$  are reported in Table 2. The  $T_{50}$  values for the most commonly studied samples, such as Printex-U and VulcanXC72R, were in close agreement with the literature data (e.g., reported  $T_{50}$  of Printex-U = 606 °C and  $T_{50}$  of VulcanXC72R = 683 °C by Atribak et al.<sup>61</sup> and reported  $T_{50}$  of Printex-U = 607 °C and  $T_{50}$  of VulcanXC72R = 667 °C by Hinot<sup>62</sup>). In general, there were three major groups in the considered samples: (i) Monarch 1300, Monarch 1400, and Printex-XE2B had low light-off temperatures ( $T_{10} < 500$  °C) and, hence, the highest oxidation rate; (ii) Printex-G, Monarch 280, VulcanXC72R, and graphite showed high light-off temperatures ( $T_{10} > 600$  °C) and, hence, the lowest oxidation rate; and (iii) all other samples had a moderate oxidation rate, with a  $T_{10}$  ranging between 500 and 600 °C. The trend was similar for  $T_{50}$  and  $T_{90}$  (see Table 2). Monarch 1300 and Monarch 1400 contained 7% moisture, as compared to

Table 2. Light-Off Temperature Data from Non-isothermal Experiments

sample number	sample name	10% O <sub>2</sub> , $\beta = 5 \text{ }^{\circ}\text{C}/\text{min}$			air, $\beta = 5 \text{ }^{\circ}\text{C}/\text{min}$		
		T <sub>10</sub> (°C)	T <sub>50</sub> (°C)	T <sub>90</sub> (°C)	T <sub>10</sub> (°C)	T <sub>50</sub> (°C)	T <sub>90</sub> (°C)
1	diesel soot	541	640	685	499	607	647
2	graphite	687	764	800	671	740	784
3	Mogul-E	548	630	663	532	601	623
4	Monarch 1300	444	562	590	444	539	550
	Monarch 1300	482 <sup>a</sup>	563 <sup>a</sup>	590 <sup>a</sup>	468 <sup>a</sup>	539 <sup>a</sup>	550 <sup>a</sup>
5	Monarch 1400	478	615	651	452	587	612
	Monarch 1400	513 <sup>a</sup>	616 <sup>a</sup>	651 <sup>a</sup>	496 <sup>a</sup>	589 <sup>a</sup>	612 <sup>a</sup>
6	Monarch 280	617	674	713	543	609	650
7	N 120	550	626	663	526	591	617
8	N 339	579	641	674	553	606	631
9	N 762	583	649	686	565	614	636
10	Printex-G	637	696	738	606	655	693
11	Printex-U	543	615	662	524	584	625
12	Printex-XE2B	479	547	589	459	512	545
13	Regal 330 R	587	659	696	559	626	651
14	Regal 400 R	565	641	675	548	612	635
15	VulcanXC72R	631	692	733	610	664	701

<sup>a</sup>Data without moisture (see the text for details).

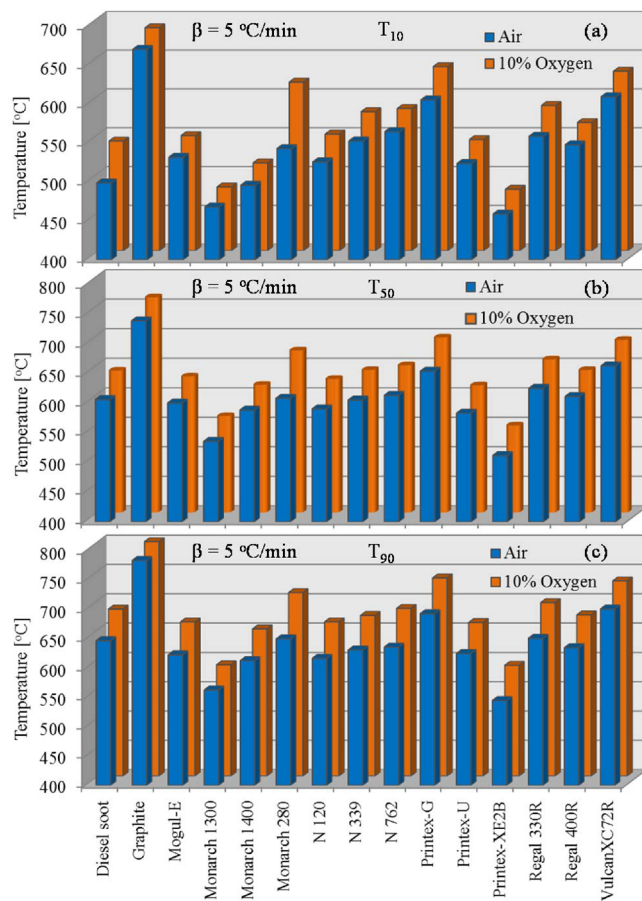


Figure 7. Comparison of T<sub>10</sub>, T<sub>50</sub>, and T<sub>90</sub> values for all samples with 10% O<sub>2</sub> and air. Oxidation is faster with air. The operating conditions are the same as in Figures 5 and 6.

negligible moisture (0–0.6%) in the other samples. Therefore, oxidation data for Monarch 1300 and Monarch 1400 are reported with and without considering the moisture content (see Table 2). To calculate the conversion without considering the moisture content, the conversion (~4–5%) of those two

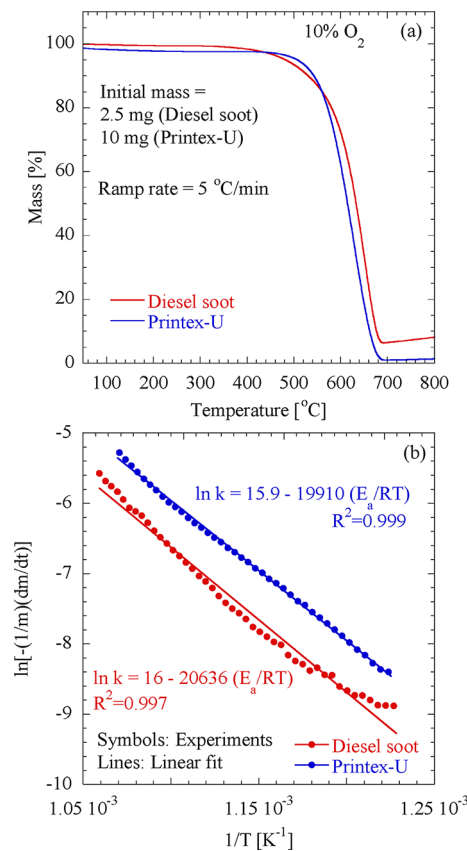


Figure 8. (a) Mass loss profiles and (b) Arrhenius plots for diesel soot and Printex-U samples using method A. The operating conditions are the same as in Figure 5.

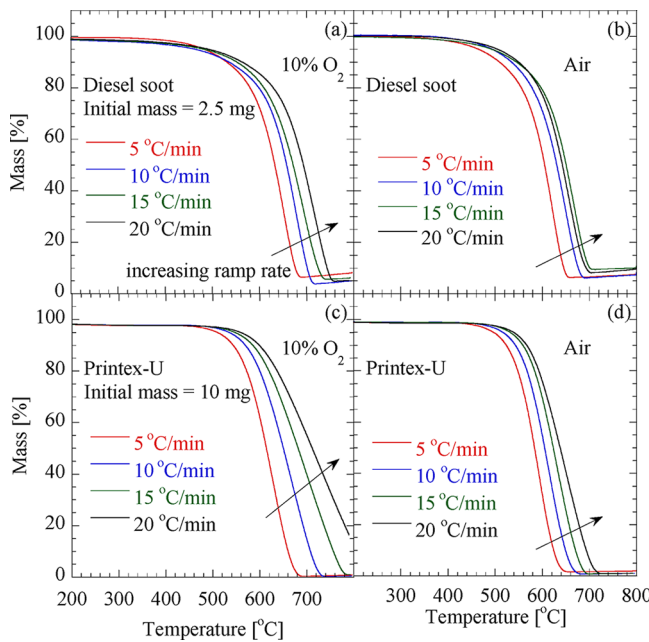
samples just before reaching 200 °C was used to compute the “corrected” initial mass without moisture. As expected, the T<sub>10</sub> values were significantly affected by the moisture content, but the T<sub>50</sub> and T<sub>90</sub> values were not.

Figure 7 compares the T<sub>10</sub>, T<sub>50</sub>, and T<sub>90</sub> values for all samples with 10% O<sub>2</sub> and air. The T<sub>10</sub>–T<sub>90</sub> values of all samples were lower in the case of oxidation with air than those with 10% O<sub>2</sub>.

**Table 3.** Apparent Kinetic Parameters from Non-isothermal and Isothermal Experiments<sup>a</sup>

		10% O <sub>2</sub>						air							
sample number	samples	range (%)	R <sup>2</sup>	E (kJ/mol)	A (Pa <sup>-1</sup> s <sup>-1</sup> )	k <sub>550</sub> (Pa <sup>-1</sup> s <sup>-1</sup> )	(Pa <sup>-1</sup> s <sup>-1</sup> )	k <sub>600</sub> (Pa <sup>-1</sup> s <sup>-1</sup> )	(Pa <sup>-1</sup> s <sup>-1</sup> )	k <sub>650</sub> (Pa <sup>-1</sup> s <sup>-1</sup> )	(Pa <sup>-1</sup> s <sup>-1</sup> )	k <sub>700</sub> (Pa <sup>-1</sup> s <sup>-1</sup> )	(Pa <sup>-1</sup> s <sup>-1</sup> )	k <sub>750</sub> (Pa <sup>-1</sup> s <sup>-1</sup> )	(Pa <sup>-1</sup> s <sup>-1</sup> )
1	diesel soot	10–90	0.991	154–172 <sup>b</sup>	1.0 × 10 <sup>2</sup> –9.4 × 10 <sup>2b</sup>	1.1 × 10 <sup>-8</sup>	4.8 × 10 <sup>-8</sup>	1.7 × 10 <sup>-7</sup>	10–90	0.985	152–169 <sup>b</sup>	1.0 × 10 <sup>2</sup> –8.5 × 10 <sup>2b</sup>	1.6 × 10 <sup>-8</sup>	6.6 × 10 <sup>-8</sup>	
		10–90	0.898	155–198 <sup>c</sup>	2.4 × 10 <sup>2</sup> –3.4 × 10 <sup>5c</sup>	2.2 × 10 <sup>-8c</sup>	8.6 × 10 <sup>-8c</sup>	2.9 × 10 <sup>-7c</sup>	10–90	0.872	121–163 <sup>c</sup>	2.3 × 10 <sup>0</sup> –5.0 × 10 <sup>2c</sup>	2.2 × 10 <sup>-8c</sup>	8.3 × 10 <sup>-8c</sup>	
		20–90	0.956	112–142 <sup>d</sup>	3.3 × 10 <sup>1</sup> –2.6 × 10 <sup>1d</sup>	2.3 × 10 <sup>-8d</sup>	6.9 × 10 <sup>-8d</sup>	1.8 × 10 <sup>-7d</sup>	20–90	0.683	133–153 <sup>d</sup>	6.2 × 10 <sup>0</sup> –1.8 × 10 <sup>2d</sup>	2.2 × 10 <sup>-8d</sup>	7.9 × 10 <sup>-8d</sup>	
2	graphite	10–80	0.995	226	3.7 × 10 <sup>4</sup>	1.7 × 10 <sup>-10</sup>	1.1 × 10 <sup>-9</sup>	5.9 × 10 <sup>-9</sup>	10–90	0.999	229	4.8 × 10 <sup>4</sup>	1.4 × 10 <sup>-10</sup>	9.6 × 10 <sup>-10</sup>	
3	Mogul-E	10–75	0.980	186	9.4 × 10 <sup>3</sup>	1.5 × 10 <sup>-8</sup>	7.0 × 10 <sup>-8</sup>	2.8 × 10 <sup>-7</sup>	10–60	0.958	214	5.9 × 10 <sup>5</sup>	1.6 × 10 <sup>-8</sup>	9.4 × 10 <sup>-8</sup>	
4	Monarch 1300	10–80	0.945	164	2.9 × 10 <sup>3</sup>	1.2 × 10 <sup>-7</sup>	4.6 × 10 <sup>-7</sup>	1.5 × 10 <sup>-6</sup>	10–80	0.870	197	4.7 × 10 <sup>5</sup>	1.5 × 10 <sup>-7</sup>	7.8 × 10 <sup>-7</sup>	
		5–80 <sup>e</sup>	0.932 <sup>e</sup>	145 <sup>e</sup>	1.9 × 10 <sup>2e</sup>	1.1 × 10 <sup>-7e</sup>	3.7 × 10 <sup>-7e</sup>	1.1 × 10 <sup>-6e</sup>	5–80 <sup>e</sup>	0.861 <sup>e</sup>	156 <sup>e</sup>	8.6 × 10 <sup>2e</sup>	1.0 × 10 <sup>-7e</sup>	4.0 × 10 <sup>-7e</sup>	
5	Monarch 1400	10–80	0.897	93–117 <sup>d</sup>	1.5 × 10 <sup>-1</sup> –1.9 × 10 <sup>1d</sup>	9.0 × 10 <sup>-8d</sup>	2.3 × 10 <sup>-7d</sup>	5.2 × 10 <sup>-7d</sup>	10–80	0.940	146	5.2 × 10 <sup>1</sup>	2.9 × 10 <sup>-8</sup>	9.7 × 10 <sup>-8</sup>	
		5–80 <sup>e</sup>	0.952 <sup>e</sup>	125 <sup>e</sup>	3.6 × 10 <sup>1</sup>	2.6 × 10 <sup>-8</sup>	8.9 × 10 <sup>-8</sup>	2.6 × 10 <sup>-7</sup>	10–80	0.940	146	5.2 × 10 <sup>1</sup>	2.9 × 10 <sup>-8</sup>	9.7 × 10 <sup>-8</sup>	
6	Monarch 280	10–90	0.989	220	2.4 × 10 <sup>5</sup>	2.6 × 10 <sup>-9</sup>	3.1 × 10 <sup>-8e</sup>	8.9 × 10 <sup>-8e</sup>	5–80 <sup>e</sup>	0.933 <sup>e</sup>	133 <sup>e</sup>	7.6 × 10 <sup>0e</sup>	2.8 × 10 <sup>-8e</sup>	8.5 × 10 <sup>-8e</sup>	
7	N 120	10–90	0.980	195	3.5 × 10 <sup>4</sup>	1.5 × 10 <sup>-8</sup>	7.6 × 10 <sup>-8</sup>	3.2 × 10 <sup>-7</sup>	10–80	0.994	180	3.8 × 10 <sup>3</sup>	1.4 × 10 <sup>-8</sup>	6.5 × 10 <sup>-8</sup>	
8	N 339	10–80	0.993	222	9.4 × 10 <sup>5</sup>	7.7 × 10 <sup>-9</sup>	4.9 × 10 <sup>-8</sup>	2.6 × 10 <sup>-7</sup>	10–80	0.991	243	2.6 × 10 <sup>7</sup>	1.0 × 10 <sup>-8</sup>	7.7 × 10 <sup>-8</sup>	
9	N 762	10–80	0.994	206	8.5 × 10 <sup>4</sup>	7.2 × 10 <sup>-9</sup>	4.0 × 10 <sup>-8</sup>	1.9 × 10 <sup>-7</sup>	10–80	0.992	257	1.3 × 10 <sup>8</sup>	6.3 × 10 <sup>-9</sup>	5.4 × 10 <sup>-8</sup>	
10	Printex-G	10–80	0.990	187	1.9 × 10 <sup>3</sup>	1.2 × 10 <sup>-9</sup>	4.9 × 10 <sup>-8</sup>	1.0 × 10 <sup>-7</sup>	10–80	0.987	207	3.8 × 10 <sup>4</sup>	2.8 × 10 <sup>-9</sup>	1.6 × 10 <sup>-8</sup>	
11	Printex-U	10–90	0.999	87–165 <sup>b</sup>	1.2 × 10 <sup>-2</sup> –8.2 × 10 <sup>2b</sup>	2.8 × 10 <sup>-8</sup>	1.1 × 10 <sup>-7</sup>	3.8 × 10 <sup>-7</sup>	10–90	0.999	143–182 <sup>b</sup>	3.8 × 10 <sup>1</sup> –1.0 × 10 <sup>4b</sup>	2.9 × 10 <sup>-8</sup>	7.5 × 10 <sup>-8</sup>	
		10–90	0.959	78–142 <sup>c</sup>	1.7 × 10 <sup>-2</sup> –3.8 × 10 <sup>1c</sup>	7.5 × 10 <sup>-8c</sup>	1.7 × 10 <sup>-7c</sup>	3.6 × 10 <sup>-7c</sup>	10–90	0.902	136–170 <sup>c</sup>	1.4 × 10 <sup>3</sup> –1.2 × 10 <sup>5c</sup>	4.0 × 10 <sup>-8c</sup>	1.5 × 10 <sup>-7c</sup>	
		20–90	0.987	107–136 <sup>d</sup>	1.2 × 10 <sup>-1</sup> –1.4 × 10 <sup>1d</sup>	2.7 × 10 <sup>-8d</sup>	7.6 × 10 <sup>-8d</sup>	1.9 × 10 <sup>-7d</sup>	20–90	0.832	135–153 <sup>d</sup>	6.2 × 10 <sup>0</sup> –1.5 × 10 <sup>2d</sup>	2.1 × 10 <sup>-8d</sup>	7.3 × 10 <sup>-8d</sup>	
12	Printex-XE2B	10–90	0.993	155	6.1 × 10 <sup>2</sup>	8.9 × 10 <sup>-8</sup>	3.2 × 10 <sup>-7</sup>	1.0 × 10 <sup>-6</sup>	10–90	0.997	196	1.1 × 10 <sup>6</sup>	4.1 × 10 <sup>-7</sup>	2.1 × 10 <sup>-6</sup>	
13	Regal 330 R	10–80	0.992	207	3.4 × 10 <sup>4</sup>	2.4 × 10 <sup>-9</sup>	1.4 × 10 <sup>-8</sup>	6.5 × 10 <sup>-8</sup>	10–80	0.984	171	1.6 × 10 <sup>3</sup>	2.2 × 10 <sup>-8</sup>	9.4 × 10 <sup>-8</sup>	
14	Regal 400 R	10–80	0.990	211	2.1 × 10 <sup>5</sup>	8.5 × 10 <sup>-9</sup>	5.0 × 10 <sup>-8</sup>	2.4 × 10 <sup>-7</sup>	10–80	0.987	249	5.8 × 10 <sup>7</sup>	9.1 × 10 <sup>-9</sup>	7.3 × 10 <sup>-8</sup>	
15	VulcanXC72R	10–90	0.988	210	1.9 × 10 <sup>4</sup>	9.3 × 10 <sup>-10</sup>	5.4 × 10 <sup>-9</sup>	2.6 × 10 <sup>-8</sup>	10–90	0.983	223	2.7 × 10 <sup>5</sup>	1.2 × 10 <sup>-8</sup>	6.5 × 10 <sup>-8</sup>	
		20–90	0.888	144–156 <sup>d</sup>	4.6 × 10 <sup>0</sup> –4.6 × 10 <sup>1d</sup>	4.1 × 10 <sup>-9d</sup>	1.5 × 10 <sup>-8d</sup>	4.6 × 10 <sup>-8d</sup>	20–90	0.903	188–223 <sup>d</sup>	2.8 × 10 <sup>3</sup> –1.6 × 10 <sup>5d</sup>	1.6 × 10 <sup>-9d</sup>	5.0 × 10 <sup>-8d</sup>	

<sup>a</sup>The kinetic parameters correspond to method A with ramp rate  $\beta$  of 5 °C/min, unless specified otherwise. <sup>b</sup>Method A was applied for different ramp rates ( $\beta = 5\text{--}20\text{ }^{\circ}\text{C}/\text{min}$ ). For the given range, the first value is for 20 °C/min experiments and the second value is for 5 °C/min experiments. <sup>c</sup>Method B: non-isothermal experiments with multiple-ramp rates. Activation energies and pre-exponential factors are given for the fractional conversion  $\alpha$  range of 0.1–0.9, whereas the rate constants  $k$  are reported for  $\alpha$  of 0.5. <sup>d</sup>Method C: isothermal experiments. Activation energies and pre-exponential factors are given for the fractional conversion  $\alpha$  range of 0.2–0.9, whereas the rate constants  $k$  are reported for  $\alpha$  of 0.5. <sup>e</sup>Without moisture (see the text for details).



**Figure 9.** Effect of the ramp rate and oxygen partial pressure on the oxidation of diesel soot (initial mass of 2.5 mg) and Printex-U (initial mass of 10 mg). Ramp rates of 5, 10, 15, and 20 °C/min are used. (a) Diesel soot with 10% O<sub>2</sub>, (b) diesel soot with air, (c) Printex-U with 10% O<sub>2</sub>, and (d) Printex-U with air. Operating conditions: non-isothermal experiment and flow rate at 60 mL/min.

Therefore, the oxidation of carbon black and soot samples with air was faster than with 10% O<sub>2</sub>. Because the oxidation profiles in Figures 5 and 6 showed similar trends for both cases, the decrease in  $T_{10} - T_{90}$  values for air was due to the higher concentration of O<sub>2</sub> in air (21%).

Method A discussed in section 3.1 was used to extract the apparent activation energies and pre-exponential factors. Figure 8 shows an example of data analysis for diesel soot and Printex-U. First, data in panel a confirmed that the oxidation behavior of diesel soot and Printex-U was quite similar, which explains why Printex-U is commonly used as a surrogate for diesel soot.<sup>30,40,42,59,63–65</sup> Second, we used a much wider range of conversion profile (from 10 to ~90%) for data analysis in panel b compared to the literature studies,<sup>42,66</sup> which ensured the validity of the estimated kinetic parameters over almost the complete oxidation process. Third, as shown in panel b, the  $\ln(-dm/dt)$  versus 1/T plots for diesel soot and Printex-U are almost straight lines with  $R^2 > 0.99$ , which agrees with the assumption of first-order kinetics. A similar analysis was conducted for all samples for both oxidizer gases (10% O<sub>2</sub> and air), and the kinetic parameters (along with the considered conversion ranges and  $R^2$  values) are reported in Table 3. Oxidation reaction rate constants at different temperatures ( $k_{550}$ ,  $k_{600}$ , and  $k_{650}$ ) are also given in Table 3 for both cases (10% O<sub>2</sub> and air), which indicated that oxidation with air was faster than with 10% O<sub>2</sub>.

In general, the range of activation energies reported in the literature for the oxidation of carbon black and soot samples is 100–300 kJ/mol.<sup>9,21,30,34,40,42,43,47,60,64,66–69</sup> However, the typically reported activation energies for diesel engine soot oxidation are in the range of 120–180 kJ/mol.<sup>30,59,60,68,70–72</sup> Neeft et al.<sup>59</sup> suggested that the activation energy increased in the following sequence: soot < activated carbon < carbon and chars < graphite, which was also observed in our experiments,

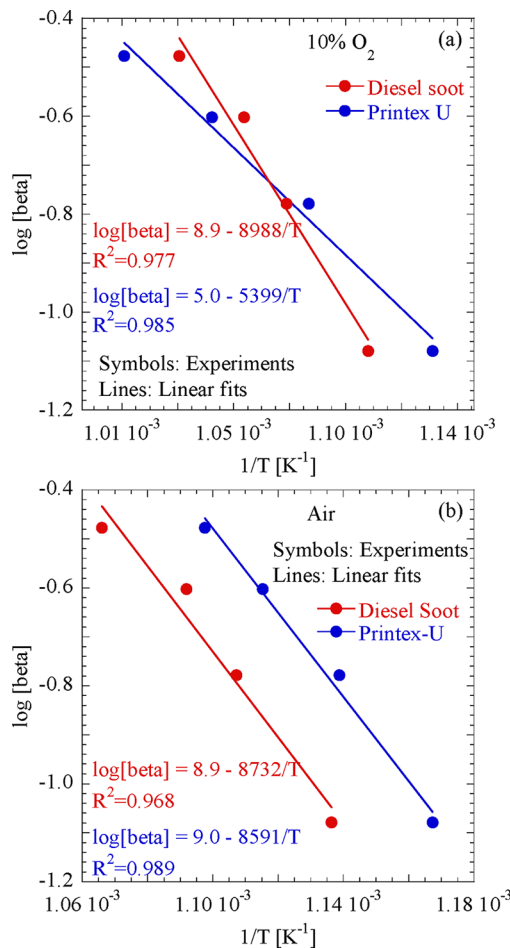


**Figure 10.** Kinetic parameter extraction for diesel soot (initial mass of 2.5 mg) and Printex-U (initial mass of 10 mg) oxidation with (a) 10% O<sub>2</sub> and (b) air using method B for a fractional conversion  $\alpha$  of 0.5. Operating conditions are the same as in Figure 9.

with graphite showing the largest activation energy and the smallest rate constant. Given the comprehensive nature of our study, literature data were not available for direct comparisons for all of the samples studied; however, the activation energies estimated from our TGA experiments were in close agreement with those reported in the literature. For example, the activation energy for diesel soot oxidation with oxygen was reported to be 164 kJ/mol by Higgins et al.<sup>60</sup> and Darcy et al.,<sup>68</sup> and 177 kJ/mol by Lee et al.,<sup>70</sup> which compare well to our estimate of 172 kJ/mol. Similarly, the activation energy for Printex-U oxidation was reported to be 168 kJ/mol by Neeft et al.<sup>59</sup> and 161 kJ/mol by Tang et al.<sup>42</sup> with 10% O<sub>2</sub> and 160 kJ/mol by Hinot<sup>62</sup> with 20% O<sub>2</sub>, which compare well with our estimates of 165 kJ/mol with 10% O<sub>2</sub> and 182 kJ/mol with air. Despite the agreement with the literature, it is important to note that the estimated kinetic parameters should ideally not change with the O<sub>2</sub> partial pressure. As alluded to earlier, this fundamental limitation most likely stems from the simplified kinetic expressions (eqs 1 and 2), where the change in the surface area during oxidation and the pore size effects were ignored and the reaction order with respect to O<sub>2</sub> was assumed to be unity. Therefore, we emphasize that the estimated activation energies (and pre-exponential factors) should be considered as apparent kinetic parameters only.

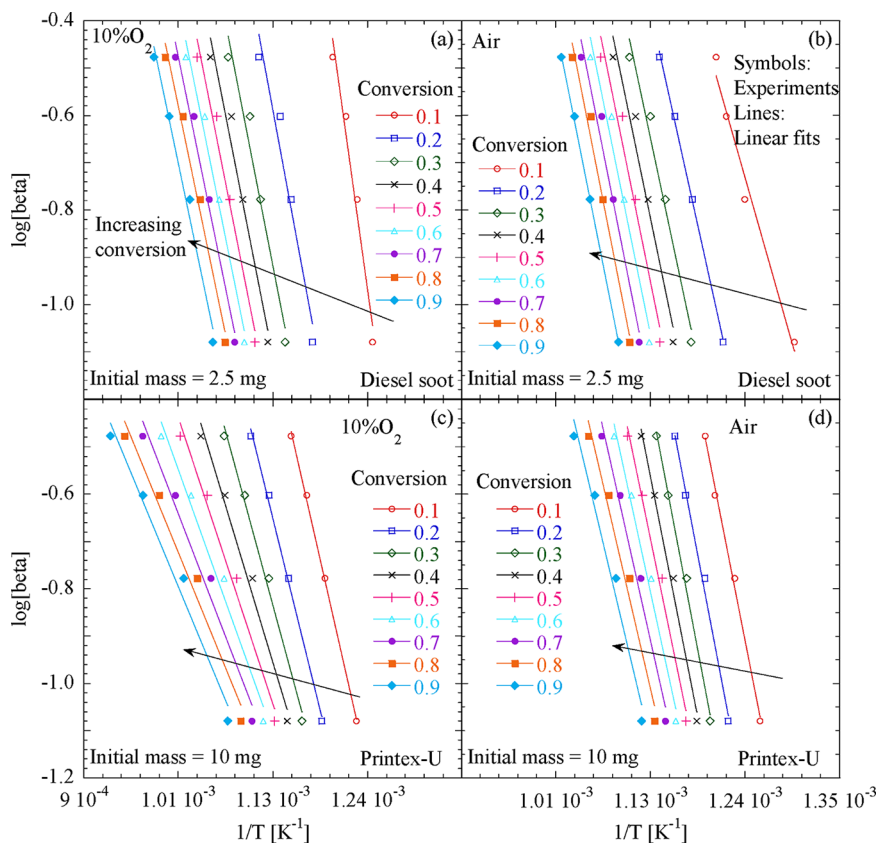


**Figure 11.** Flynn–Wall–Ozawa plot for diesel soot (initial mass of 2.5 mg) and Printex U (initial mass of 10 mg) oxidation. (a) Diesel soot with 10% O<sub>2</sub>, (b) diesel soot with air, (c) Printex-U with 10% O<sub>2</sub>, and (d) Printex-U with air, using method B for a fractional conversion  $\alpha$  range of 0.1–0.9. Operating conditions are the same as in Figure 9.

To understand the variation of the oxidation rate for the different carbon black and soot samples, they were characterized using scanning electron microscopy (SEM) and Brunauer–Emmett–Teller (BET) surface area.<sup>73</sup> SEM analysis indicated that the average particle size (over ~200 particles) varied over a wide range (20.9–74 nm). Similarly, the BET surface area varied over a wide range as well (43–1005 m<sup>2</sup>/g). The oxidation rate of carbon black and soot samples is a complex function of various structural factors and operating conditions; however, the large variations in average particle size and surface area may be used to explain some of the trends in the oxidation rate.<sup>73</sup> Monarch 1400, Monarch 1300, and Printex-XE2B had the smallest average particle size (20.9–26.7 nm), whereas Printex-G, Monarch 280, and Mogul-E had the largest particle size (69.7–74 nm). Surface areas of Monarch 1400, Monarch 1300, and Printex-XE2B were in the higher range of 342–1005 m<sup>2</sup>/g, whereas those of Printex-G, Monarch 280, and Mogul-E were in the lower range of 45–49 m<sup>2</sup>/g. The higher rate of Monarch 1400, Monarch 1300, and Printex-XE2B ( $T_{50}^{\text{O}_2}$  range of 547–616 °C) could be attributed to the smaller particle size and higher surface area. Similarly, the lower rate of Printex-G, Monarch 280, and Mogul-E ( $T_{50}^{\text{O}_2}$  range of 630–674 °C) could be attributed to the larger particle size and lower surface area.

**4.2. Effect of the Ramp Rate.** The ramp rate  $\beta$  is another operating parameter that typically shows a large impact on the oxidation profile.<sup>20,30</sup> To validate the activation energies estimated in the previous section, we conducted TGA experiments with 10% O<sub>2</sub> and air using four ramp rates (5, 10, 15, and 20 °C/min) for diesel soot and Printex-U samples. Experimental protocol details are provided in Table 1. As shown in

Figure 9, the oxidation rate shifted to higher temperatures with an increase in the ramp rate. A higher ramp rate reduces the overall reaction time in an experiment for a given temperature range, and less mass loss occurs at the same temperature point compared to a lower ramp rate case.<sup>31</sup> For example, for heating from 600 to 800 °C, it takes only 10 min with 20 °C/min, whereas it takes 40 min with 5 °C/min. Kalogirou and Samaras suggested that the higher ramp rates could also be associated with diffusional limitations, which are more prominent in the case of low oxygen concentrations.<sup>30</sup> Our experimental results with different ramp rates and oxygen partial pressures were consistent with this observation. For example, when the 10% O<sub>2</sub> versus air profiles in Figure 9 are compared, the delay in the oxidation rate with an increased ramp rate was higher for 10% O<sub>2</sub> compared to that for air. This also justifies the 5 °C/min ramp rate used in section 4.1 (method A) for kinetic parameter estimation. On the other hand, data analysis presented in this section could be affected by diffusional limitations to some extent at higher ramp rates but provide a reasonably good validation of the kinetic parameters.

Results obtained from diesel soot and Printex-U oxidation with 10% O<sub>2</sub> and air for various ramp rates (5–20 °C/min) were analyzed using method B discussed in section 3.2. Figure 10 shows a plot of log  $\beta$  versus 1/T for diesel soot and Printex-U for both 10% O<sub>2</sub> (panel a) and air (panel b) for a selected fractional conversion  $\alpha$  of 0.5. The estimated kinetic parameters are reported in Table 3. With 10% O<sub>2</sub>, the estimated activation energies for diesel soot and Printex-U oxidation were in the range of 155–198 and 78–142 kJ/mol, respectively (these ranges were based on applying method B at different fractional conversions),

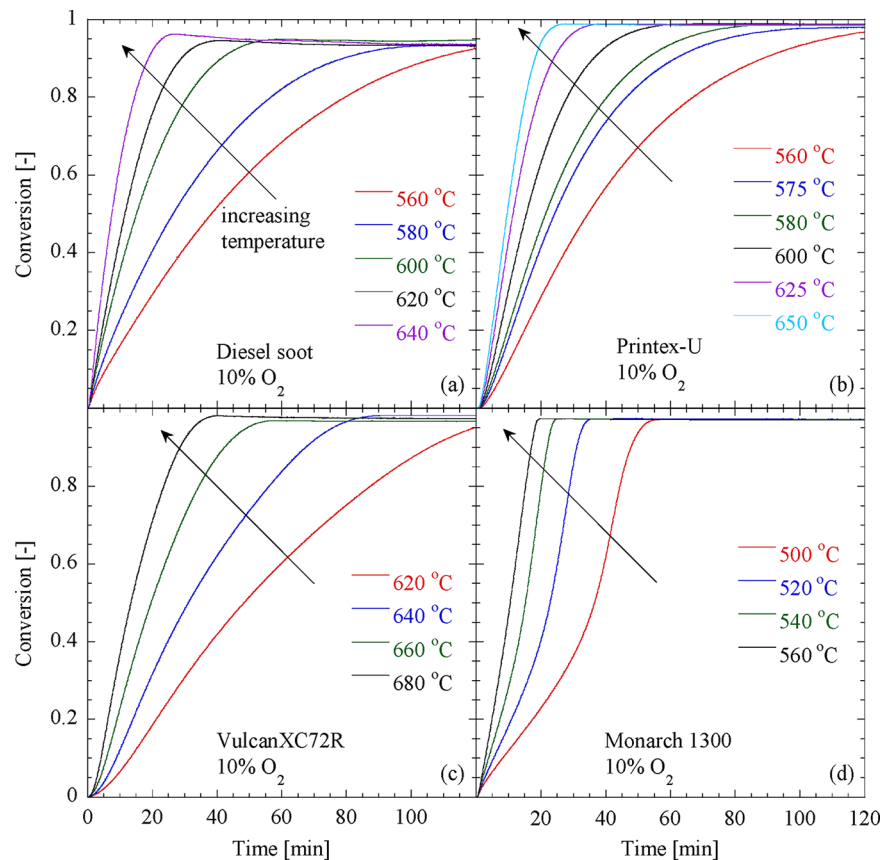


**Figure 12.** Isothermal conversion profiles of (a) diesel soot (initial mass of 2.5 mg), (b) Printex-U (initial mass of 10 mg), (c) VulcanXC72R (initial mass of 5 mg), and (d) Monarch 1300 (initial mass of 12 mg). Operating conditions: isothermal experiment, 10% O<sub>2</sub> oxidant, flow rate at 60 mL/min, and ramp rate to reach isothermal temperature at 20 °C/min.

which were comparable to the numbers estimated from method A (154–172 and 87–165 kJ/mol, respectively; these ranges were based on applying method A at different ramp rates). Similarly, with air, the estimated activation energies for diesel soot and Printex-U oxidation were in the range of 121–163 and 136–170 kJ/mol, respectively (these ranges were based on applying method B at different fractional conversions), which were also comparable to the numbers estimated from method A (152–169 and 143–182 kJ/mol, respectively; these ranges were based on applying method A at different ramp rates). A larger deviation was observed in the case of 10% O<sub>2</sub> than air, which could be due to the diffusional limitations associated with larger ramp rates and a low oxygen concentration. However, the rate constants calculated using method B at any particular temperature (see  $k$  values in Table 3 for  $\alpha = 0.5$ ) showed excellent agreement with the rate constants calculated using method A.

Before moving on to the isothermal experiments in the next section, we note that the kinetic parameters estimated using method B are dependent upon the fractional conversion  $\alpha$ . For example, parameter estimation analysis was carried out for a wider range of fractional conversion values ( $\alpha = 0.1–0.9$ ), as shown in Figure 11 for diesel soot and Printex-U. The activation energies varied with the fractional conversion (diesel soot, 155–198 kJ/mol for 10% O<sub>2</sub> and 121–163 kJ/mol for air; Printex-U, 78–142 kJ/mol for 10% O<sub>2</sub> and 136–170 kJ/mol for air). Overall, the analysis based on method B provided excellent validation for the kinetic parameters estimated using method A.

Nonetheless, we recommend experiments with lower ramp rates to avoid any influence of heat- and mass-transfer limitations.

## 5. KINETICS FROM ISOTHERMAL TESTS

Apart from the non-isothermal experiments reported thus far, we also conducted isothermal tests for selected samples (diesel soot, Printex-U, Monarch 1300, and VulcanXC72R) to further validate the kinetic parameters. The four samples were selected to cover the range from low to high oxidation rates from the non-isothermal experiments. For each sample, we conducted isothermal experiments at multiple temperature points with the same initial mass. After reaching the set point (isothermal temperature), the sample was kept at the set point for 2 h. Experimental protocol details are provided in Table 1. Method C discussed in section 3.3 was used for the analysis of the isothermal experiments.

Figure 12 shows the mass loss profiles of the four selected samples. Plots of conversion  $\alpha$  versus time  $t$  suggest that the reaction profiles or kinetic curves of diesel soot and commercial carbon black samples are of the decelerating type, in which the rate is maximum at the beginning and decreases continuously with the extent of conversion.<sup>18</sup> Reaction order models are generally used for gas–solid reactions of the decelerating type. First-order reaction kinetics was used for the analysis of these data to extract the kinetic parameters, consistent with the methods A and B discussed earlier. The estimated kinetic parameters are reported in Table 3.

In general, the activation energies estimated using method C (isothermal) were slightly lower than those estimated using

methods A and B (non-isothermal). Similarly, the pre-exponential factors calculated using method C (isothermal) were lower than those estimated using methods A and B (non-isothermal). On the other hand, the reaction rate constants computed at 550, 600, and 650 °C for  $\alpha$  of 0.5 showed good agreement with the corresponding rate constants estimated from the non-isothermal experiments. This indicated that the activation energies estimated using method C could be affected by the compensation effect between activation energies and pre-exponential factors. The compensation effect is a commonly reported phenomenon, in which change in the activation energy is compensated by change in the pre-exponential factor.<sup>28,74–76</sup> Analysis conducted at different fractional conversion values for diesel soot oxidation with 10% O<sub>2</sub> and air is shown in Figure 13a. The activation

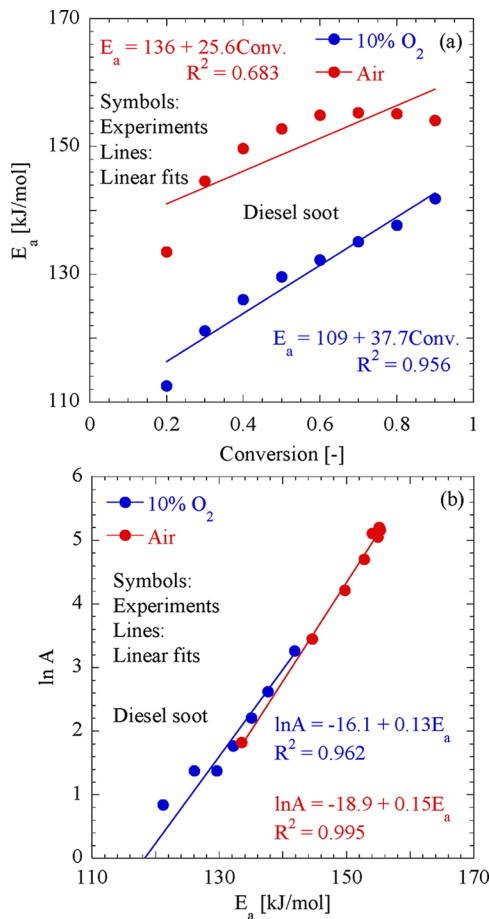


**Figure 13.** Isothermal kinetics of diesel soot oxidation using method C. (a) Variation of the activation energy with fractional conversion  $\alpha$  (range of 0.2–0.9) using both 10% O<sub>2</sub> and air. (b) Compensation effect of activation energies and pre-exponential factors. Operating conditions are the same as in Figure 12.

energy varied with fractional conversion, consistent with literature reports on solid-state reaction kinetics.<sup>18,76–78</sup> For example, the estimated activation energy ranged over fractional conversion  $\alpha$  of 0.2–0.9 for diesel soot (112–142 kJ/mol for 10% O<sub>2</sub> and 133–155 kJ/mol for air) and Printex-U (107–136 kJ/mol for 10% O<sub>2</sub> and 135–153 kJ/mol for air), and corresponding variation in pre-exponential factors confirmed the existence of the compensation effect. Figure 13b shows the variation in activation energy with the pre-exponential factor. Complex or multiple-step reaction kinetics of soot oxidation was ruled out because of the absence of multiple peaks and/or shoulders in the reaction rate curve.<sup>18</sup>

Despite this limitation, method C (isothermal) provided a reasonably good validation of the kinetic parameters estimated using methods A and B (non-isothermal).

To verify the assumption of first-order kinetics with respect to O<sub>2</sub>, we estimated the reaction order ( $n_{O_2}$ ) based on the isothermal experiments with 10% O<sub>2</sub> and air for the four samples studied here (diesel soot, Printex-U, Monarch 1300, and VulcanXC72R). The estimated  $n_{O_2}$  was 1 for diesel soot, whereas it was close to 1 for the other carbon black samples (0.95 for Printex-U, 0.88 for Monarch 1300, and 0.90 for VulcanXC72R). Finally, to demonstrate the validity of effective models used here, Figure 14 shows how the apparent kinetic

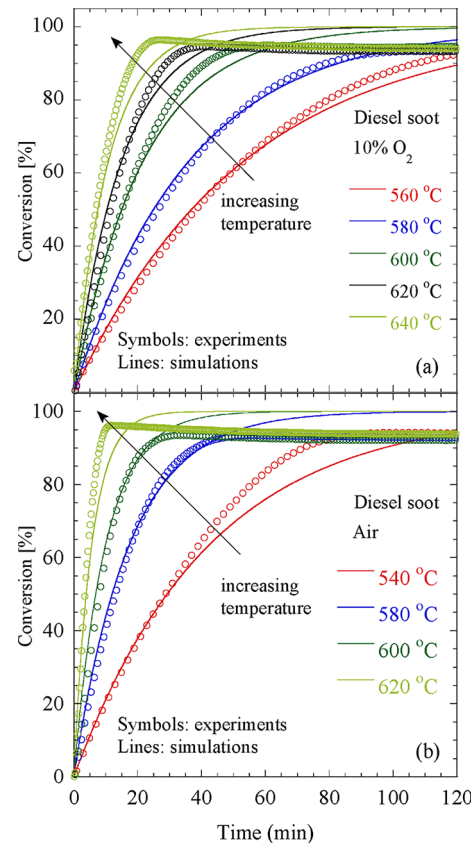


**Figure 14.** Validation of estimated apparent kinetic parameters and the effective model against experimental results in Figure 12a and also against isothermal experiments with air. Simulations were conducted using apparent activation energies and pre-exponential factors at fractional conversion  $\alpha$  of 0.5 from the isothermal experiments for diesel soot with (a) 10% O<sub>2</sub> and (b) air. A reaction order  $n_{O_2}$  of 1 was used. Diesel soot showed incomplete conversion in the experiments because of the presence of metal oxides and ash particles.

parameters extracted at nominal conditions (fractional conversion  $\alpha = 0.5$ ) along with first-order kinetics with respect to O<sub>2</sub> can adequately capture the entire range of experimental data; i.e., the compensation effect between the apparent activation energy and pre-exponential factors was not critical for the effective models considered here.

## 6. CONCLUSION

In this work, we conducted non-isothermal and isothermal TGA experiments for more than a dozen carbon black samples and a diesel engine soot sample with 10% O<sub>2</sub> and air to

investigate the effect of operating conditions on the oxidation rate and to extract the corresponding apparent kinetic parameters. Limitations associated with the availability of oxygen were avoided by conducting experiments in sufficient oxidizer gas flow rate conditions. The partial pressure of oxygen and ramp rates showed significant effects on the oxidation rate. Oxidation with air was faster than with 10% O<sub>2</sub>, because of the higher concentration of oxygen in air. The activation energy for the oxidation of carbon black samples ranged from 125 to 257 kJ/mol, whereas that for soot oxidation was ~155 kJ/mol. Oxidation rate trends were explained on the basis of structural characteristics, such as SEM-based average particle size and BET surface area. In general, a low particle size and high surface area were associated with a higher oxidation rate and vice versa. Kinetic parameters extracted using the non-isothermal experiments at a single-ramp rate (method A) were further validated using additional non-isothermal experiments with multiple-ramp rates (method B) and isothermal experiments (method C). The overall agreement for kinetic parameters estimated using the three methods (consisting of separately conducted experiments) was remarkable; however, the analysis in methods B and C indicated that the extracted parameters could be affected by a compensation effect between activation energies and pre-exponential factors as they change with the extent of conversion. Overall, the comprehensive understanding developed in this work for oxidation of carbon black and soot samples could be beneficial for the improved design and optimization of DPF operation and regeneration protocols.

## AUTHOR INFORMATION

### Corresponding Author

\*Telephone: 1-443-523-8609 . Fax: 1-860-486-2959. E-mail: ashish.mhadeshwar@gmail.com.

### Notes

The authors declare no competing financial interest.

## ACKNOWLEDGMENTS

This work was supported by Corning, Inc. and the Department of Energy (DOE) through Award DE-EE0003226 ("Improving Reliability and Durability of Efficient and Clean Energy Systems"). Hom N. Sharma also acknowledges the Department of Education GAANN Fellowship for funding. The authors thank Laura Pinatti from the Institute of Materials Science (IMS) at the University of Connecticut for access to the TGA equipment.

## REFERENCES

- (1) Schneider, C. G.; Hill, L. B. *Diesel and Health in America: The Lingering Threat*; Clean Air Task Force: Boston, MA, 2005; [http://www.catf.us/resources/publications/files/Diesel\\_Health\\_in\\_America.pdf](http://www.catf.us/resources/publications/files/Diesel_Health_in_America.pdf).
- (2) U.S. Energy Information Administration (EIA). *Diesel Fuel Explained—Use of Diesel*; EIA: Washington, D.C., 2011; [http://www.eia.gov/energyexplained/index.cfm?page=diesel\\_use](http://www.eia.gov/energyexplained/index.cfm?page=diesel_use) (accessed Feb 5, 2012).
- (3) California Energy Commission. *Petroleum Watch*; California Energy Commission: Sacramento, CA, 2011; [http://energyalmanac.ca.gov/petroleum/petroleum\\_watch/2011-09-16\\_Petroleum\\_Watch.pdf](http://energyalmanac.ca.gov/petroleum/petroleum_watch/2011-09-16_Petroleum_Watch.pdf) (accessed Feb 5, 2012).
- (4) Bensaid, S.; Caroca, C. J.; Russo, N.; Fino, D. *Can. J. Chem. Eng.* **2011**, *89* (2), 401–407.
- (5) Prasad, R.; Bella, V. R. *Bull. Chem. React. Eng. Catal.* **2010**, *5* (2), 69–86.
- (6) Fino, D. *Sci. Technol. Adv. Mater.* **2007**, *8* (1–2), 93–100.
- (7) Xi, J.; Zhong, B. *J. Chem. Eng. Technol.* **2006**, *29* (6), 665–673.
- (8) Vander Wal, R. L.; Bryg, V. M.; Hays, M. D. *J. Aerosol Sci.* **2010**, *41* (1), 108–117.
- (9) Yezers, A.; Currier, N. W.; Kim, D. H.; Eadler, H. A.; Epling, W. S.; Peden, C. H. F. *Appl. Catal., B* **2005**, *61* (1–2), 120–129.
- (10) Jones, C. C.; Chughtai, A. R.; Murugaverl, B.; Smith, D. M. *Carbon* **2004**, *42* (12–13), 2471–2484.
- (11) Clague, A. D. H.; Donnet, J. B.; Wang, T. K.; Peng, J. C. M. *Carbon* **1999**, *37* (10), 1553–1565.
- (12) Prasad, R.; Bella, V. R. *Bull. Chem. React. Eng. Catal.* **2010**, *5* (2), 95–101.
- (13) Hoyer, M.; Foureman, G.; Valcovic, L.; Grant, L.; McGrath, J.; Koppikar, A.; Pepelko, W.; Chen, C.; Ris, C. *Health Assessment Document for Diesel Engine Exhaust*; United States Environmental Protection Agency (U.S. EPA): Washington, D.C., 2002; <http://www.epa.gov/ttn/atw/dieselfinal.pdf> (accessed March 14, 2012).
- (14) United States Environmental Protection Agency (U.S. EPA). *National Ambient Air Quality Standards (NAAQS)*; U.S. EPA: Washington, D.C., 2011; <http://epa.gov/air/criteria.html> (accessed Jan 12, 2012).
- (15) Ecopoint, Inc. *Emissions Standards*; Ecopoint, Inc.: Mississauga, Ontario, Canada, 2011; <http://www.dieselnet.com/standards/eu/hd.php> (accessed Feb 15, 2012).
- (16) Williams, S. Surface intermediates, mechanism, and reactivity of soot oxidation. Ph.D. Thesis, University of Toronto, Toronto, Ontario, Canada, 2008.
- (17) Maricq, M. *J. Aerosol Sci.* **2007**, *38* (11), 1079–1118.
- (18) Vyazovkin, S.; Burnham, A. K.; Criado, J. M.; Pérez-Maqueda, L. A.; Popescu, C.; Sbirrazzuoli, N. *Thermochim. Acta* **2011**, *520* (1–2), 1–19.
- (19) Song, J.; Alam, M.; Boehman, A. L. *Combust. Sci. Technol.* **2007**, *179* (9), 1991–2037.
- (20) Rodriguez-Fernandez, J.; Oliva, F.; Vazquez, R. A. *Energy Fuels* **2011**, *25* (5), 2039–2048.
- (21) Kalogirou, M.; Samaras, Z. *J. Therm. Anal. Calorim.* **2010**, *99* (3), 1005–1010.
- (22) López-Fonseca, R.; Elizundia, U.; Landa, I.; Gutiérrez-Ortiz, M. A.; González-Velasco, J. R. *Appl. Catal., B* **2005**, *61* (1–2), 150–158.
- (23) Zouaoui, N.; Brilhac, J.; Mechati, F.; Jeguirim, M.; Djellouli, B.; Gilot, P. *J. Therm. Anal. Calorim.* **2010**, *102* (3), 837–849.
- (24) Neeft, J. P. A.; Hoornaert, F.; Makkee, M.; Moulijn, J. A. *Thermochim. Acta* **1996**, *287* (2), 261–278.
- (25) Gilot, P.; Bonnefoy, F.; Marcuccilli, F.; Prado, G. *Combust. Flame* **1993**, *95* (1–2), 87–100.
- (26) Stanmore, B. R.; Gilot, P. *Thermochim. Acta* **1995**, *261*, 151–164.
- (27) Gilot, P.; Brillard, A.; Stanmore, B. R. *Combust. Flame* **1995**, *102* (4), 471–480.
- (28) Khawam, A.; Flanagan, D. R. *J. Pharm. Sci.* **2006**, *95* (3), 472–498.
- (29) Liu, C.; Yu, J.; Sun, X.; Zhang, J.; He, J. *Polym. Degrad. Stab.* **2003**, *81* (2), 197–205.
- (30) Kalogirou, M.; Samaras, Z. *J. Therm. Anal. Calorim.* **2009**, *98* (1), 215–224.
- (31) Castaldi, M. J.; Kwon, E. Thermo-gravimetric analysis (TGA) of combustion and gasification of styrene–butadiene copolymer (SBR). *Proceedings of the 13<sup>th</sup> North American Waste to Energy Conference*; Orlando, FL, May 23–25, 2005; NAWTEC13-3149.
- (32) Costache, M. C.; Wang, D.; Heidecker, M. J.; Manias, E.; Wilkie, C. A. *Polym. Adv. Technol.* **2006**, *17*, 272–280.
- (33) Gašparovič, L.; Koreňová, Z.; Jelemenský, L'. Kinetic study of wood chips decomposition by TGA. *Proceedings of the 36<sup>th</sup> International Conference of Slovak Society of Chemical Engineering*; Tatranské Matliare, Slovakia, May 25–29, 2009; p 178.
- (34) López-Fonseca, R.; Landa, I.; Elizundia, U.; Gutiérrez-Ortiz, M. A.; González-Velasco, J. R. *Combust. Flame* **2006**, *144* (1–2), 398–406.
- (35) Skreiberg, A.; Skreiberg, Ø.; Sandquist, J.; Sørum, L. *Fuel* **2011**, *90* (6), 2182–2197.

- (36) Ollero, P.; Serrera, A.; Arjona, R.; Alcantarilla, S. *Fuel* **2002**, *81* (15), 1989–2000.
- (37) López-Fonseca, R.; Landa, I.; Elizundia, U.; Gutiérrez-Ortiz, M. A.; González-Velasco, J. R. *Chem. Eng. J.* **2007**, *129* (1–3), 41–49.
- (38) Gómez-Barea, A.; Ollero, P.; Arjona, R. *Fuel* **2005**, *84* (12–13), 1695–1704.
- (39) Brilhac, J. F.; Bensouda, F.; Gilot, P.; Brillard, A.; Stanmore, B. *Carbon* **2000**, *38* (7), 1011–1019.
- (40) Stanmore, B. R.; Brilhac, J. F.; Gilot, P. *Carbon* **2001**, *39* (15), 2247–2268.
- (41) Stanmore, B.; Gilot, P.; Prado, G. *Thermochim. Acta* **1994**, *240*, 79–89.
- (42) Tang, J.; Song, Q.; He, B.; Yao, Q. *Sci. China, Ser. E: Technol. Sci.* **2009**, *S2* (6), 1535–1542.
- (43) Yezzerets, A.; Currier, N. W.; Eadler, H. A.; Suresh, A.; Madden, P. F.; Branigin, M. A. *Catal. Today* **2003**, *88* (1–2), 17–25.
- (44) López-Fonseca, R.; Landa, I.; Gutiérrez-Ortiz, M. A.; González-Velasco, J. R. *J. Therm. Anal. Calorim.* **2005**, *80* (1), 65–69.
- (45) Leistner, K.; Nicolle, A.; Berthout, D.; da Costa, P. *Combust. Flame* **2012**, *159* (1), 64–76.
- (46) Salvador, S.; Commandré, J. M.; Stanmore, B. R. *Fuel* **2003**, *82* (6), 715–720.
- (47) Hartman, J. R.; Beyler, A. P.; Riahi, S.; Beyler, C. L. *Fire Mater.* **2012**, *36* (3), 177–184.
- (48) Yang, S.; Lee, K.; Chong, H. *SAE Tech. Pap. Ser.* **2010**, DOI: 10.4271/2010-01-2166.
- (49) Flynn, J. H.; Wall, L. A. *J. Polym. Sci., Polym. Phys.* **1966**, *4* (5), 323–328.
- (50) Ozawa, T. *Bull. Chem. Soc. Jpn.* **1965**, *38* (11), 1881–1886.
- (51) Li, Y.; Xu, L.; Yao, X.; Luo, T.; Li, G. *J. Phys.: Conf. Ser.* **2012**, *339* (1), 1–8.
- (52) Chen, X.; Yu, J.; Guo, S. *J. Appl. Polym. Sci.* **2007**, *103* (3), 1978–1984.
- (53) Doyle, C. D. *Nature* **1965**, *207* (4994), 290–291.
- (54) Doyle, C. D. *J. Appl. Polym. Sci.* **1961**, *5* (15), 285–292.
- (55) Azambre, B.; Collura, S.; Darcy, P.; Trichard, J. M.; Da Costa, P.; García-García, A.; Bueno-López, A. *Fuel Process. Technol.* **2011**, *92* (3), 363–371.
- (56) Tighe, C. J.; Twigg, M. V.; Hayhurst, A. N.; Dennis, J. S. *Combust. Flame* **2012**, *159* (1), 77–90.
- (57) Kalogirou, M.; Pistikopoulos, P.; Ntziachristos, L.; Samaras, Z. *J. Therm. Anal. Calorim.* **2009**, *95* (1), 141–147.
- (58) Neeft, J. P. A.; Makkee, M.; Moulijn, J. A. *Fuel Process. Technol.* **1996**, *47* (1), 1–69.
- (59) Neeft, J. P. A.; Nijhuis, T. X.; Smakman, E.; Makkee, M.; Moulijn, J. A. *Fuel* **1997**, *76* (12), 1129–1136.
- (60) Higgins, K. J.; Jung, H.; Kittelson, D. B.; Roberts, J. T.; Zachariah, M. R. *J. Phys. Chem. A* **2002**, *96* (1), 96–103.
- (61) Atribak, I.; Bueno-López, A.; García-García, A. *Combust. Flame* **2010**, *157* (11), 2086–2094.
- (62) Hinot, K. Catalytic soot oxidation by platinum on sintered metal filters: Influence of the platinum quantity, particle size and location, and investigation of the platinum–soot contact. Ph.D. Thesis, Universität Karlsruhe, Karlsruhe, Germany, 2006.
- (63) Setiabudi, A.; Makkee, M.; Moulijn, J. A. *Appl. Catal., B* **2004**, *50* (3), 185–194.
- (64) Wang-Hansen, C.; Kamp, C. J.; Skoglundh, M.; Andersson, B.; Carlsson, P. *J. Phys. Chem. C* **2011**, *115* (32), 16098–16108.
- (65) Jung, H.; Kittelson, D. B.; Zachariah, M. R. *Combust. Flame* **2004**, *136* (4), 445–456.
- (66) Stratakis, G. A.; Stamatelos, A. M. *Combust. Flame* **2003**, *132* (1–2), 157–169.
- (67) Du, Z.; Sarofim, A. F.; Longwell, J. P.; Mims, C. A. *Energy Fuels* **1991**, *5* (1), 214–221.
- (68) Darcy, P.; Da Costa, P.; Mellottée, H.; Trichard, J.; Djégamariadassou, G. *Catal. Today* **2007**, *119* (1–4), 252–256.
- (69) Messerer, A.; Niessner, R.; Pöschl, U. *Carbon* **2006**, *44* (2), 307–324.
- (70) Lee, J.; Lee, H.; Song, S.; Chun, K. *SAE Tech. Pap. Ser.* **2007**, DOI: 10.4271/2007-01-1270.
- (71) Otto, K.; Sieg, M.; Zinbo, M.; Bartosiewicz, L. *SAE Tech. Pap. Ser.* **1980**, DOI: 10.4271/1980-02-01.
- (72) Fredrik Ahlström, A.; Ingemar Odenbrand, C. U. *Carbon* **1989**, *27* (3), 475–483.
- (73) Pahalagedara, L. R.; Sharma, H. N.; Kuo, C.; Dharmarathna, S.; Joshi, A. V.; Suib, S. L.; Mhadeshwar, A. B., *submitted to Energy & Fuels*, **2012**.
- (74) Galwey, A. K. *Thermochim. Acta* **2003**, *399* (1–2), 1–29.
- (75) Galwey, A. K.; Brown, M. E. *Thermochim. Acta* **1997**, *300* (1–2), 107–115.
- (76) Vyazovkin, S.; Wight, C. A. *Annu. Rev. Phys. Chem.* **1997**, *48* (1), 125–149.
- (77) Vyazovkin, S. *Int. Rev. Phys. Chem.* **2000**, *19* (1), 45–60.
- (78) Vyazovkin, S.; Sbirrazzuoli, N. *Macromol. Rapid Commun.* **2006**, *27* (18), 1515–1532.
- (79) TA Instruments. Q500 Series Thermogravimetric Analyzer; TA Instruments: New Castle, DE, 2012; <http://www.tainstruments.com/product.aspx?id=20&n=1&siteid=11> (accessed March 22, 2012).